Inorganic Chemistry
Article
Cite This: Inorg. Chem. XXXX, XXX, XXX−XXX
pubs.acs.org/IC

Preferential Adsorption of CO_2 in an Ultramicroporous MOF with Cavities Lined by Basic Groups and Open-Metal Sites

Shyamapada Nandi,[†] Rahul Maity,[†] Debanjan Chakraborty,[†] Hemkalyan Ballav,[†] and Ramanathan Vaidhyanathan*[,†,‡]

[†]Department of Chemistry, Indian Institute of Science Education and Research, Dr. Homi Bhabha Rd., Pashan, Pune, 411008, India
[‡]Centre for Energy Science, Indian Institute of Science Education and Research, Dr. Homi Bhabha Rd., Pashan, Pune, 411008, India

Supporting Information

ABSTRACT: Here, we present a new ultramicroporous Cu_2 paddle-wheel based MOF. This ultramicroporous MOF has most of the features such as porosity (BET surface area = 945 m^2/g), CO_2 capacity (3.5 mmol/g at ambient temperature and pressure), CO_2/N_2 selectivity (sCO_2/N_2 = 250), and fast CO_2 diffusion kinetics ($D_c = 2.25 \times 10^{-9}$ m^2/s), comparable to some of the other high-performing ultramicroporous MOFs, with strong binding sites. Typically, such MOFs exhibit strong CO_2−framework interactions (evidenced from a heat of adsorption ≥ 38 kJ/mol). However, the MOF explained here, despite having channels lined by the amine and the open-metal sites, possesses only a moderate CO_2−framework interaction (HOA = 26 kJ/mol). Using periodic DFT, we have probed this counterintuitive observation.

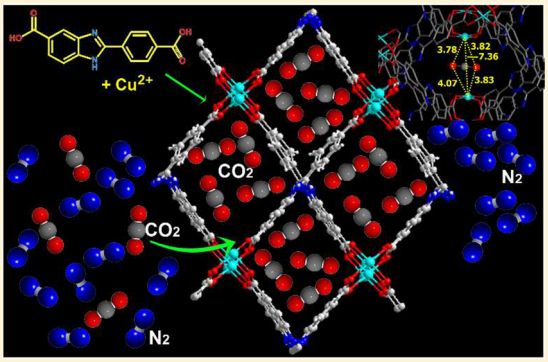

INTRODUCTION

Carbon dioxide (CO_2) is a key heat-trapping gas responsible for global warming through the greenhouse effect.[1] Capturing CO_2 from industrial sources will have marked impact on their global concentrations.[2] Pre and postcombustion CO_2 capture are two efficient technologies for such large-scale captures.[3] They are carried out using pressure and temperature swing adsorption (P/TSA) methods,[4] which prove to be extremely energy efficient.[5,6] Typically, such capture processes employ solid sorbents which physisorb CO_2.[6a] However, implementation of these large-scale CO_2 capture technology requires substantial cost reduction. This can be achieved by modifying the engineering aspects of the process. But more prospects lie in developing superior sorbents.[6b]

Current industrial scrubbers are zeolites with high molecular-sieving capability.[7] In this regard, Metal−Organic Frameworks (MOFs) have attracted significant attention due to their high structural tunability, CO_2 capacity, selectivity, and faster kinetics as well as low regeneration/parasitic energy.[8−11] MOFs can be chemically manipulated to adsorb CO_2 selectively at low partial pressures, a property that is critical for the postcombustion CO_2 capture. Ultramicroporous MOFs (UM-MOFs) (pore size < 6 Å) built from rigid short linkers with basic character are suitable for selective CO_2 capture. The high selectivity arises from enhanced framework−CO_2 and cooperative CO_2···CO_2 interactions.[8c] Such molecular level interactions define the optimal heat of adsorption, which gets expressed as the ease of CO_2 regeneration.[11c] Enormous efforts are being invested in identifying and optimizing the framework−CO_2 interactions in MOFs.[12] Some of the most energetic framework−CO_2 interactions are amine−CO_2 interaction,[8c,12a−c] open-metal−CO_2 interaction,[12d,e] aromatic π cloud−CO_2 interaction,[11b,12f] and organic functional group−CO_2 interaction.[12g,h] Understanding the adsorption sites of high-performing MOFs is vital for the future design of superior sorbents. De facto, MOFs provide an excellent crystalline platform for understanding such critical gas−solid interactions.

Herein, we report a 2D Cu based ultramicroporous MOF (IISERP-MOF20) built from 2-(4-carboxyphenyl)-1*H*-benzo[*d*]imidazole-5-carboxylate. It shows moderate CO_2 uptake as well as CO_2/N_2 selectivity for flue gas compositions at room temperature. Also, this MOF exhibits an optimal Heat of Adsorption (HOA) for CO_2 which further ensures the low regeneration energy demand. However, the observed HOA is quite low considering that the channels are lined with both basic groups and bare metal sites, which are known to interact strongly with CO_2. To investigate this oddity, we simulated the different binding sites in the MOF using Grand Canonical Monte Carlo (GCMC) methods. Notably, some unique CO_2−metal interactions are identified, which deviate from the previously observed ones.

EXPERIMENTAL SECTION

The organic linker, with basic character and metal-binding carboxylate groups, was synthesized via a simple condensation reaction between aldehyde and 1,2-diamine (Scheme 1). The dicarboxylic acid, 2-(4-carboxyphenyl)-1*H*-benzo[*d*]imidazole-5-carboxylic acid (LH_2) was synthesized by reacting 4-formyl benzoic acid and 3,4-diaminobenzoic

Received: February 3, 2018

DOI: 10.1021/acs.inorgchem.8b00304
Inorg. Chem. XXXX, XXX, XXX−XXX

Scheme 1. Schematic Representation of the Synthesis of 2-(4-Carboxyphenyl)-1*H*-benzo[*d*]imidazole-5-carboxylic Acid

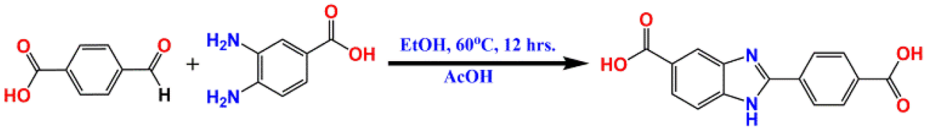

acid in the presence of acetic acid at 60 °C for 12 h. The LH_2 was obtained as a yellowish off-white powder in over 80% yield.

$Cu(L)(H_2O)\cdot(DMF)_{1.5}(EtOH)_{1.5}$, IISERP-MOF20, was synthesized via a solvothermal reaction between copper nitrate and 2-(4-carboxyphenyl)-1*H*-benzo[*d*]imidazole-5-carboxylic acid in a solution containing dimethylformamide, ethanol, and water at 80 °C for 36 h. The product, blue-colored square-shaped platy crystals, was obtained in ∼74% yield (based on Cu).

RESULTS AND DISCUSSION

Single crystal X-ray structure analysis reveals that IISERP-MOF20 crystallizes in an orthorhombic system (a = 20.8093(11) Å; b = 9.7634(5) Å; c = 25.2583(11) Å; Sp. Gr. *Cmca*). The structure consists of typical Cu_2 paddlewheel units, where the Cu-Cu dimers get connected by four different 2-(4-carboxyphenyl)-1*H*-benzo[*d*]imidazole-5-carboxylate ligands (Figure S5). Each Cu is penta-coordinated. Among the five coordinations, four are satisfied by oxygen atoms of the carboxylate unit and the fifth one is satisfied by a water molecule. These Cu_2 paddlewheel nodes are extended by four ligand units into a 2D layer along the **ac** plane with large near square-shaped apertures (16.21 × 16.21 Å, shown with green lines in Figures 1 and S7). The adjacent layers are shifted by half-a-unit cell along the a and c directions and are rotated by 90°, giving a staggered ABAB... arrangement (Figure S8). This positions the five-membered heteroatomic rings of the benzimidazole unit from the adjacent layer right at the edges of the square aperture and the Cu_2 paddlewheel from the adjacent layers above and below the center of the square aperture in the middle layer. Now, for each square shown (in green) in Figure 1, there are four N-containing five-membered rings at the edges which hydrogen bond above and below the plane, thus forming a column of N−H···N hydrogen bonds (N···H−N = 2.0137 Å). These are vital in holding the 2D layers together into a stable 3D framework. Also, the Cu_2 paddlewheels from alternate layers run as a column along the b direction. The half-unit cell shift in the adjacent layers thus compartmentalizes the large aperture in each paddlewheel derived layer into four smaller pores, creating a rhombic channel of dimensions 7.63 × 7.63 Å (not factoring the van der Waals radii, Figure 1 and Figure S7).

In fact, the overall 3D structure is held together by the covalent bonds between metal and the ligand in the *ac* plane and by the hydrogen bond interactions running along the perpendicular b direction. Removal of the coordinated water molecules generates two open-metal sites at each paddlewheel unit, and the open-metal sites from the adjacent A-A layers in the ABAB stacking line up at a distance of 7.36(3) Å. A PLATON analysis suggests a 48.7% potential solvent accessible void present in the structure. A squeeze refinement drastically improves the R-factor, indicating the presence of disordered solvent molecules. Unfortunately, a successful modeling of these electron densities as solvents was not possible. However, we have assigned the electron counts from the squeeze analysis to 1.5 DMF and 1.5 EtOH molecules per unit cell, and this

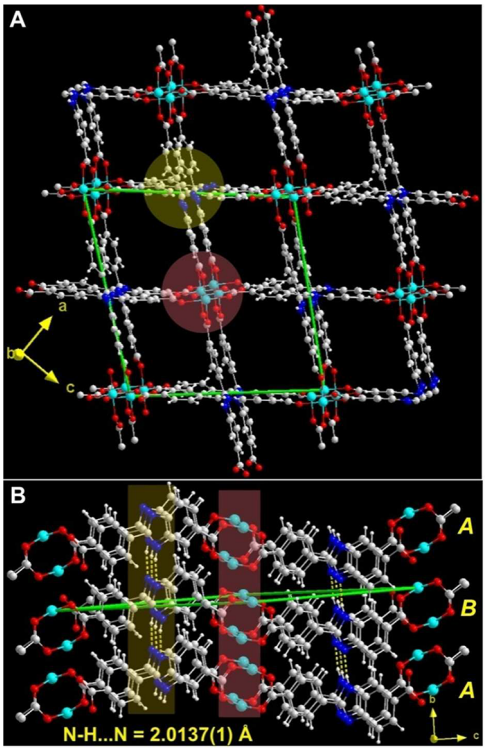

Figure 1. (A) Three-dimensional structure of the IISERP-MOF20 formed by the ABAB... stacking of the Cu_2 paddlewheel based layers. The green line is a guide for the eye to see the large square-shaped aperture formed in each layer. Yellow and maroon circles show the nodes present in the structure. (B) The column of interlayer N−H···N hydrogen bonds between the nitrogens of the five-membered rings of the benzimidazole units and the column of Cu_2 paddlewheels is shown (Cu···Cu = 7.36 Å).

matches well with the solvent composition calculated from the TGA analysis.

For a practical large-scale industrial CO_2 capture process, the sorbents are required in tonnes. Hence, even in a laboratory scale, it is worthwhile to demonstrate the MOF synthesis in grams. In this regard, making MOFs using a single metal and a single ligand can be advantageous (Scheme S1). Here, the IISERP-MOF20 was synthesized in gram scale by merely scaling up the constituents from the mg scale synthesis, and the purity was confirmed via Powder X-ray Diffraction (PXRD) analysis as presented in Figures 2A and S9−S10. From TGA, the MOF was found to be stable up to 260 °C (Figure S12). The N_2 adsorption at 77 K confirms the permanent porosity of the MOF (Figure 2B). A Brunauer−Emmett−Teller (BET) fit obtained using the adsorption branch of the 77 K N_2 isotherm yields a surface area of 945 m^2/g (Figure S14), which is quite high for an ultramicroporous MOF.[8c,f,11a] Nonlocalized Density Functional Theory (NLDFT) fit yields a pore diameter of 5.85 Å, which matches extremely well with the pore size (inset, Figure 2B and Figure S15). Notably, this ultramicroporous MOF adsorbs a good amount of CO_2 (3.5 mmol/g) at 1 bar

DOI: 10.1021/acs.inorgchem.8b00304
Inorg. Chem. XXXX, XXX, XXX−XXX

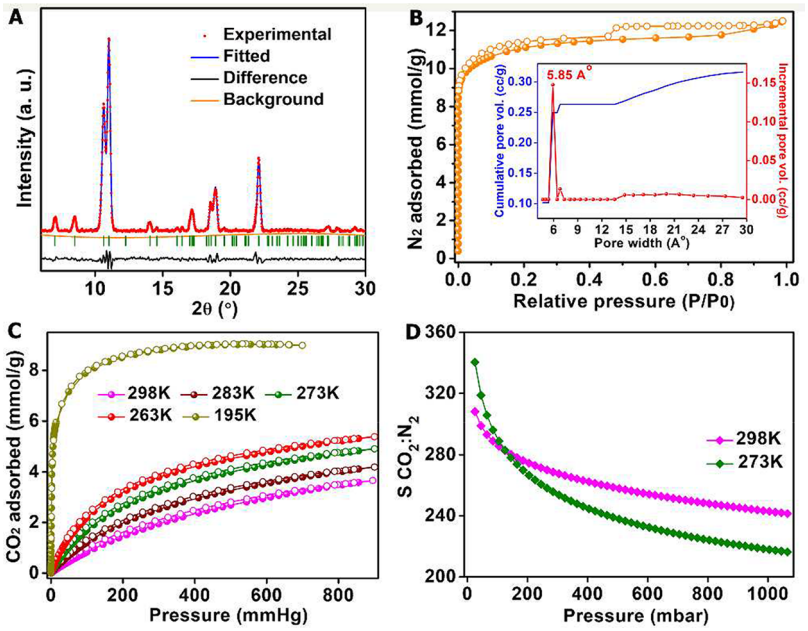

Figure 2. (A) A Pawley fit to the PXRD of the desolvated sample showing the bulk purity (the as-synthesized sample shows additional solvent sensitive peaks; see Figure S9). (B) The 77 K N_2 isotherm of IISERP-MOF20. The inset shows the pore size distribution. (C) CO_2 sorption isotherms of IISERP-MOF20 at different temperatures. (D) CO_2/N_2 selectivity of IISERP-MOF20 calculated using IAST model employing a nominal composition of $15CO_2$:$85N_2$.

and 298 K (Figure 2C) and has a saturation CO_2 capacity of 9.0 mmol/g (195 K CO_2 isotherm). However, it shows less N_2 uptake at room temperature. The Ideal Adsorption Solution Theory (IAST) calculation performed using the isotherms collected at 273 and 298 K, employing a nominal composition of $15CO_2$:$85N_2$, yields a CO_2/N_2 selectivity of 220 and 250, respectively (Figures 2D and S16). Although the selectivity values are not as high as those of the recently reported UM-MOFs,[8f,11a] these are sufficient to achieve the benchmarked 99% purity during separation.[13]

The HOA calculated using both virial and DFT models employing the 298, 283, 273, and 263 K CO_2 isotherms was 26 kJ/mol at zero loading. At higher loadings, the HOA reaches values of 20−22 kJ/mol (Figures 3A and S17). Such moderate HOA (25−35 kJ/mol) suggests facile regeneration.[11c] A cycling experiment further confirmed this.

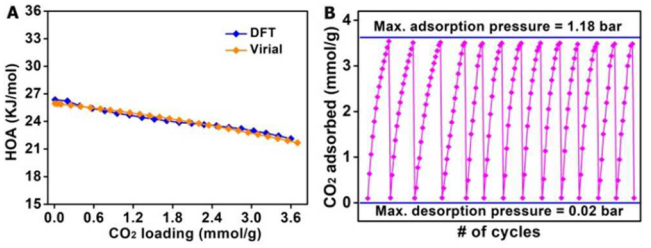

Figure 3. (A) HOA as a function of CO_2 loading calculated using DFT and virial models. (B) CO_2 adsorption−desorption cycles at room temperature.

As can be seen from the Figure 3B, the CO_2 uptake remains almost the same even after 14 cycles. Also, the CO_2 sorption is very smooth, suggesting smooth diffusion of CO_2 in the MOF. Diffusion kinetics was determined using a Rate of Adsorption (ROA) analysis at 273 K. The average diffusion coefficient (D_c) for CO_2 within the pores of IISERP-MOF20 was calculated to be 2.25×10^{-9} m^2/s (Figure S19). This diffusion coefficient is comparable to what was observed for the recently reported 1D porous Ni-PyC MOF[11a] and is higher than that observed in some of the other MOFs with similar or larger pores such as MOF-5 (1.17×10^{-9} m^2/s) or MOF-177 (1.17×10^{-9} m^2/s).[14] It is worth mentioning that the D_c observed for IISERP-MOF20 is at least 2 orders of magnitude higher than that for zeolite-13X,[14c] the current industrial CO_2 scrubber.

Considering that the activated MOF consists of appropriately oriented open-metal sites and basic secondary amine groups, the observed moderate HOAs were puzzling. We have used simulations to probe this. For this, the number of CO_2 molecules (saturation capacity from 195 K adsorption) for a $2 \times 2 \times 2$ cell was calculated to be 200. These many CO_2's were allowed to diffuse into the cell freely. From which, the most probable positions for CO_2 inside the structure were identified using the simulated annealing method embedded in the Materials Studio program (see the Supporting Information). The observed CO_2 positions provide some useful information. As shown in Figure 4A, even in the lowest energy configurations, the majority of the CO_2 molecules preferred the middle of the pore despite having open-metal sites and secondary amine groups lining the channels. Also, the adjacent CO_2 molecules were separated by distances in the range of 3.4−4.7 Å (Figures 4B and S21). Weak intermolecular dispersive interactions operate at such distances.[8c] Some of the CO_2 molecules arrange themselves into a typical T-shaped configuration where the $\delta-$ oxygen of one CO_2 interacts with the $\delta+$ carbon of another CO_2 molecule (Figures 4B and S21). This T-shaped configuration among CO_2 molecules is quite common in solid phase CO_2.[15] All of these results are consistent with our previous reports.[8c] But the surprising observation comes from the orientation of the CO_2 molecules that reside proximal to the open-metal sites (Figure 4C). Typically, the CO_2 molecules interact with the open-metal sites via M···O($\delta-$)=C($\delta+$)=O($\delta-$) (head-on interaction, M···O

DOI: 10.1021/acs.inorgchem.8b00304
Inorg. Chem. XXXX, XXX, XXX−XXX

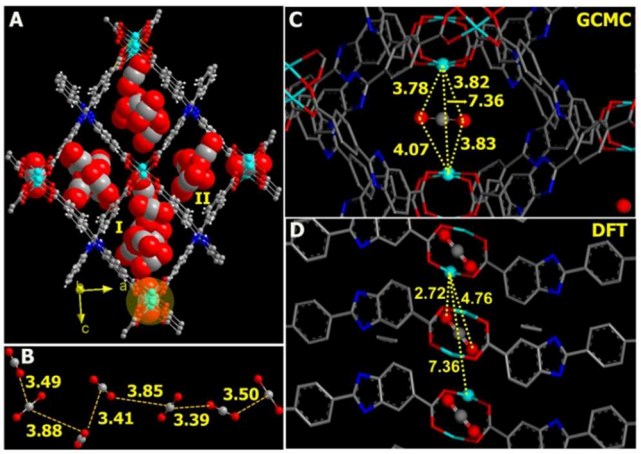

Figure 4. (A) CO_2 positions from GCMC simulations. (B) Interactions and distances between CO_2 molecules in the pore labeled as I. (C) A specific CO_2 sandwiched between the open-metal sites. Note: The other CO_2 molecules in the pore have not been shown for clarity. (D) Lowest energy configuration from periodic DFT for a sandwiched/pillaring CO_2, calculated without including any other CO_2 molecules in the pore.

distance = ~2.4 Å).[16] In contrast, in our case, the CO_2 molecules align parallel to the open-metal sites and get sandwiched between two open-metal sites from the alternate layers. This enables the CO_2 oxygens to interact weakly, but equally, with both the metal sites (Figure 4C) and simultaneously with the other proximal CO_2 molecules in the pore.

To emphasize the role of $CO_2\cdots CO_2$ cooperative interactions and to evaluate the feasibility of the pillaring CO_2 to get activated at this open-metal sites separation, we carried out further DFT simulations. For this, as an initial model, we positioned a CO_2 molecule to pillar the Cu_2 paddlewheels with the oxygens of the CO_2 interacting in a head-on fashion with the metal (Cu···O═C═O = 2.46 Å; O═C = 1.22 Å). The 2.46 Å is as per the value available in the literature for the strongest head-on interaction with the open-metal site.[16] No other CO_2 molecules were included. We optimized the geometry using a periodic DFT (CASTEP program), with a constraint on the metal−organic layers (to retain the coordinates from the single crystal XRD, Cu−Cu distance = 7.36 Å).

At this separation, this CO_2 molecule does not remain perpendicular; instead, it tilts by an angle of ~53° (about the mean plane) and the Cu···O═C═O distance equilibrates to 2.72 Å and the O═C to 1.18 Å (Figure 4D). This explains that, for the CO_2 to be strongly activated, the interlayer separation needs to be even shorter. But the N−H···N hydrogen bonds keep the layers away at a distance of 7.36 Å, thus decreasing the polarization of the CO_2 molecules by the open-metal sites. It is noteworthy that this distance (Cu···O═C═O = 2.72 Å) is different from the distance observed from the GCMC routine as in this case the cooperative effects from the other CO_2 molecules in the pores were not included. In fact, considering the mere moderate HOA (22−26 kJ/mol), the parallel to mean-plane orientation observed from the GCMC simulations seems to be the most probable. Also, this orientation most probably gets stabilized by the cooperative interactions between the CO_2 molecules in the pore. For a CO_2 to act as a pillar between the two open-metal sites and to get activated (high HOA), the metal−metal separation needs to be <7.3 Å and there have to be cooperative interactions from other directions within a pore to place the trapped CO_2 molecule in such a perfectly linear pillaring position. In our case, the two potentially strong interacting sites, the open-metal site and the basic groups, compete for the same CO_2 and their orientations do not seem to support any mutual cooperativity. This is similar to one of our earlier observations, where the high density of amine functional groups becomes mutually antagonistic, hindering their interactions with the adsorbed CO_2 molecules.[17]

CONCLUSIONS

Here, we have a Cu-MOF with favorable CO_2 capture characteristics. However, despite having pores functionalized simultaneously with a bare-metal site and basic benzimidazole functionality, it shows only a moderately strong interaction with CO_2. The positions and the orientations observed for CO_2 within these pores indicate that these two strong adsorption sites compete among them for the same CO_2. It emphasizes that, when it comes to improving the CO_2 interactions by trapping cooperatively aggregated CO_2's via strong binding functionalities, their mutual orientation becomes crucial to gain a synergistic advantage.

ASSOCIATED CONTENT

Supporting Information

The Supporting Information is available free of charge on the ACS Publications website at DOI: 10.1021/acs.inorgchem.8b00304.

The synthetic and experimental details (PDF)

Accession Codes

CCDC 1577174 contains the supplementary crystallographic data for this paper. These data can be obtained free of charge via www.ccdc.cam.ac.uk/data_request/cif, or by emailing data_request@ccdc.cam.ac.uk, or by contacting The Cambridge Crystallographic Data Centre, 12 Union Road, Cambridge CB2 1EZ, UK; fax: +44 1223 336033.

AUTHOR INFORMATION

Corresponding Author

*E-mail: vaidhya@iiserpune.ac.in.

ORCID

Ramanathan Vaidhyanathan: 0000-0003-4490-4397

Notes

The authors declare no competing financial interest.

ACKNOWLEDGMENTS

We acknowledge IISER-Pune and the MHRD-FAST program for the necessary funding. S.N. thanks DST, SERB, and IISER-Pune for the fellowship.

REFERENCES

(1) (a) https://climate.nasa.gov/vital-signs/carbon-dioxide/. (b) United States Environmental Protection Agency. *Inventory of U.S. Greenhouse Gas Emissions and Sinks: 1990−2015*; EPA: Washington, DC, 2017. (c) Keith, D. W. Why capture CO_2 from the atmosphere? *Science* **2009**, *325*, 1654−1655.

(2) Rochelle, G. T. Amine scrubbing for CO_2 capture. *Science* **2009**, *325*, 1652−1654.

(3) (a) Herm, Z. R.; Swisher, J. A.; Smit, B.; Krishna, R.; Long, J. R. Metal−Organic Frameworks as adsorbents for hydrogen purification

DOI: 10.1021/acs.inorgchem.8b00304
Inorg. Chem. XXXX, XXX, XXX−XXX

and precombustion carbon dioxide capture. *J. Am. Chem. Soc.* **2011**, *133*, 5664−1567. (b) Samanta, A.; Zhao, A.; Shimizu, G. K. H.; Sarkar, P.; Gupta, R. Post-combustion CO_2 capture using solid sorbents: a review. *Ind. Eng. Chem. Res.* **2012**, *51*, 1438−1463.

(4) (a) Sircar, S.; Golden, T. C. Purification of hydrogen by pressure swing adsorption. *Sep. Sci. Technol.* **2000**, *35*, 667−687. (b) Ciferno, J. P.; Fout, T. E.; Jones, A. P.; Murphy, J. T. Capturing carbon from existing coal-fired power plant. *Chem. Eng. Prog.* **2009**, *105*, 33−41.

(5) Raksajati, A.; Ho, M. T.; Wiley, D. E. Reducing the cost of CO_2 capture from flue gases using aqueous chemical absorption. *Ind. Eng. Chem. Res.* **2013**, *52*, 16887−16901.

(6) (a) Lin, L.-C.; Berger, A. H.; Martin, R. L.; Kim, J.; Swisher, J. A.; Jariwala, K.; Rycroft, C. H.; Bhown, A. S.; Deem, M. W.; Haranczyk, M.; Smit, B. In silico screening of carbon-capture materials. *Nat. Mater.* **2012**, *11*, 633−641. (b) Patel, H. A.; Byun, J.; Yavuz, C. T. Carbon dioxide capture adsorbents: chemistry and methods. *ChemSusChem* **2017**, *10*, 1303−1317. (c) Chakraborty, A.; Laha, S.; Kamali, K.; Eswaramoorthy, M.; Narayana, C.; Maji, T. K. In Situ Growth of Self-assembled ZIF-8-Aminoclay Nanocomposites with Enhanced Surface Area and CO_2 Uptake. *Inorg. Chem.* **2017**, *56*, 9426−9435.

(7) Ko, D.; Siriwardane, R.; Biegler, L. T. Optimization of a pressure-swing adsorption process using zeolite 13X for CO_2 sequestration. *Ind. Eng. Chem. Res.* **2003**, *42*, 339−348.

(8) (a) Huck, J. M.; Lin, L.-C.; Berger, A. H.; Shahrak, M. N.; Martin, R. L.; Bhown, A. S.; Haranczyk, M.; Reuter, K.; Smit, B. Evaluating different classes of porous materials for carbon capture. *Energy Environ. Sci.* **2014**, *7*, 4132−4146. (b) Mason, J. A.; Sumida, K.; Herm, Z. R.; Krishna, R.; Long, J. R. Evaluating metal−organic frameworks for post-combustion carbon dioxide capture via temperature swing adsorption. *Energy Environ. Sci.* **2011**, *4*, 3030−3040. (c) Vaidhyanathan, R.; Iremonger, S. S.; Shimizu, G. K. H.; Boyd, P. G.; Alavi, S.; Woo, T. K. Direct observation and quantification of CO_2 binding within an amine-functionalized nanoporous solid. *Science* **2010**, *330*, 650−653. (d) Zhang, Z.; Yao, Z.-Z.; Xiang, S.; Chen, B. Perspective of microporous metal−organic frameworks for CO_2 capture and separation. *Energy Environ. Sci.* **2014**, *7*, 2868−2899. (e) Liao, P.-Q.; Chen, X. W.; Liu, S.-Y.; Li, X.-Y.; Xu, Y.-T.; Tang, M.-N.; Rui, Z. B.; Ji, H.-B.; Zhang, J.-P.; Chen, X.-M. Putting an ultrahigh concentration of amine groups into a metal−organic framework for CO_2 capture at low pressures. *Chem. Sci.* **2016**, *7*, 6528−6533. (f) Nugent, P.; Belmabkhout, Y.; Burd, S. D.; Cairns, A. J.; Luebke, R.; Forrest, K.; Pham, T.; Ma, S.; Space, B.; Wojtas, L.; Eddaoudi, M.; Zaworotko, M. J. Porous materials with optimal adsorption thermodynamics and kinetics for CO_2 separation. *Nature* **2013**, *495*, 80−84. (g) Gao, Q.; Xu, J.; Cao, D.; Chang, Z.; Bu, X.-H. A Rigid Nested Metal−Organic Framework Featuring a Thermoresponsive Gating Effect Dominatedby Counterions. *Angew. Chem., Int. Ed.* **2016**, *55*, 15027−15030.

(9) (a) Xiang, S.; He, Y.; Zhang, Z.; Wu, H.; Zhou, W.; Krishna, R.; Chen, B. Microporous metal-organic framework with potential for carbon dioxide capture at ambient conditions. *Nat. Commun.* **2012**, *3*, 954. (b) Fracaroli, A. M.; Furukawa, H.; Suzuki, M.; Dodd, M.; Okajima, S.; Gándara, F.; Reimer, J. A.; Yaghi, O. M. Metal−organic frameworks with precisely designed interior for carbon dioxide capture in the presence of water. *J. Am. Chem. Soc.* **2014**, *136*, 8863−8866. (c) Bhatt, P. M.; Belmabkhout, Y.; Cadiau, A.; Adil, K.; Shekhah, O.; Shkurenko, A.; Barbour, L. J.; Eddaoudi, M. A fine-tuned fluorinated MOF addresses the needs for trace CO_2 removal and air capture using physisorption. *J. Am. Chem. Soc.* **2016**, *138*, 9301−9307. (d) Liu, J.; Tian, J.; Thallapally, P. K.; McGrail, B. P. Selective CO_2 capture from flue gas using metal−organic frameworks a fixed bed study. *J. Phys. Chem. C* **2012**, *116*, 9575−9581. (e) Kumar, A.; Hua, C.; Madden, D. G.; O'Nolan, D.; Chen, K.-J.; Keane, L.-A. J.; Perry, J. J., IV; Zaworotko, M. J. Hybrid ultramicroporous materials (HUMs) with enhanced stability and trace carbon capture performance. *Chem. Commun.* **2017**, *53*, 5946−5949. (f) Adil, K.; Belmabkhout, Y.; Pillai, R. S.; Cadiau, A.; Bhatt, P. M.; Assen, A. H.; Maurin, G.; Eddaoudi, M. Gas/vapour separation using ultra-microporous metal−organic frameworks: insights into the structure/separation relationship. *Chem. Soc. Rev.* **2017**, *46*, 3402−3430.

(10) (a) Yang, Q.; Vaesen, S.; Ragon, F.; Wiersum, A. D.; Wu, D.; Lago, A.; Devic, T.; Martineau, C.; Taulelle, F.; Llewellyn, P. L.; Jobic, H.; Zhong, C.; Serre, C.; De Weireld, G.; Maurin, G. A Water Stable Metal−Organic Framework with optimal Features for CO_2 Capture. *Angew. Chem., Int. Ed.* **2013**, *52*, 10316−10320. (b) Sanchez-Gonzalez, E.; Gonzalez-Zamora, E.; Martínez-Otero, D.; Jancik, V.; Ibarra, I. A. Bottleneck Effect of N,N-Dimethylformamide in InOF-1: Increasing CO_2 Capture in Porous Coordination Polymers. *Inorg. Chem.* **2017**, *56*, 5863−5872. (c) Nguyen, P. T. K.; Nguyen, H. T. D.; Pham, H. Q.; Kim, J.; Cordova, K. E.; Furukawa, H. Synthesis and Selective CO_2 Capture Properties of a Series of Hexatopic Linker-Based Metal−Organic Frameworks. *Inorg. Chem.* **2015**, *54*, 10065−10072. (d) Sharma, V.; De, D.; Saha, R.; Das, R.; Chattaraj, P. K.; Bharadwaj, P. K. A Cu(II)-MOF capable of fixing CO_2 from air and showing high capacity H_2 and CO_2 adsorption. *Chem. Commun.* **2017**, *53*, 13371−13374. (e) Zhang, S.-M.; Chang, Z.; Hu, T.-L.; Bu, X.-H. New Three-Dimensional Porous Metal Organic Framework with Tetrazole Functionalized Aromatic Carboxylic Acid: Synthesis, Structure, and Gas Adsorption Properties. *Inorg. Chem.* **2010**, *49*, 11581−11586. (f) Chen, Y.-Q.; Qu, Y.-K.; Li, G.-R.; Zhuang, Z.-Z.; Chang, Z.; Hu, T.-L.; Xu, J.; Bu, X.-H. Zn(II)-Benzotriazolate Clusters Based Amide Functionalized Porous Coordination Polymers with High CO_2 Adsorption Selectivity. *Inorg. Chem.* **2014**, *53*, 8842−8844.

(11) (a) Nandi, S.; Collins, S.; Chakraborty, D.; Banerjee, D.; Thallapally, P. K.; Woo, T. K.; Vaidhyanathan, R. Ultralow parasitic energy for postcombustion CO_2 capture realized in a nickel isonicotinate metal−organic framework with excellent moisture stability. *J. Am. Chem. Soc.* **2017**, *139*, 1734−1737. (b) Nandi, S.; De Luna, P.; Daff, T. D.; Rother, J.; Liu, M.; Buchanan, W.; Hawari, A. I.; Woo, T. K.; Vaidhyanathan, R. A single-ligand ultra-microporous MOF for precombustion CO_2 capture and hydrogen purification. *Sci. Adv.* **2015**, *1*, e1500421. (c) Simmons, J. M.; Wu, H.; Zhou, W.; Yildirim, T. Carbon capture in metal−organic frameworks-a comparative study. *Energy Environ. Sci.* **2011**, *4*, 2177−2185.

(12) (a) Lin, J. B.; Zhang, J.-P.; Chen, X. M. Nonclassical active site for enhanced gas sorption in porous coordination polymer. *J. Am. Chem. Soc.* **2010**, *132*, 6654−6656. (b) Demessence, A.; D'Alessandro, D. M.; Foo, M. L.; Long, J. R. Strong CO_2 binding in a water-stable, triazolate-bridged metal−organic framework functionalized with ethylenediamine. *J. Am. Chem. Soc.* **2009**, *131*, 8784−8786. (c) Pal, A.; Chand, S.; Das, M. C. A Water-Stable Twofold Interpenetrating Microporous MOF for Selective CO_2 Adsorption and Separation. *Inorg. Chem.* **2017**, *56*, 13991−13997. (d) Poloni, R.; Lee, K.; Berger, R. F.; Smit, B.; Neaton, J. B. Understanding trends in CO_2 adsorption in metal−organic frameworks with open-metal sites. *J. Phys. Chem. Lett.* **2014**, *5*, 861−865. (e) Das, M. C.; Xiang, S.; Zhang, Z.; Chen, B. Functional mixed metal−organic frameworks with metalloligands. *Angew. Chem., Int. Ed.* **2011**, *50*, 10510−10520. (f) Yang, L.; Chang, G.; Wang, D. High and selective carbon dioxide capture in nitrogen-containing aerogels via synergistic effects of electrostatic in-plane and dispersive $\pi-\pi$-stacking interactions. *ACS Appl. Mater. Interfaces* **2017**, *9*, 15213−15218. (g) Lee, H. M.; Youn, I. S.; Saleh, M.; Lee, J. W.; Kim, K. S. Interactions of CO_2 with various functional molecules. *Phys. Chem. Chem. Phys.* **2015**, *17*, 10925−10933. (h) Collins, S. P.; Daff, T. D.; Piotrkowski, S. S.; Woo, T. K. Materials design by evolutionary optimization of functional groups in metal-organic frameworks. *Sci. Adv.* **2016**, *2*, e1600954.

(13) Chung, Y. G.; Gómez-Gualdrón, D. A.; Li, P.; Leperi, K. T.; Deria, P.; Zhang, H.; Vermeulen, N. A.; Stoddart, J. F.; You, F.; Hupp, J. T.; Farha, O. K.; Snurr, R. Q. In silico discovery of metal-organic frameworks for precombustion CO_2 capture using a genetic algorithm. *Sci. Adv.* **2016**, *2*, e1600909.

(14) (a) Saha, D.; Bao, Z.; Jia, F.; Deng, S. Adsorption of CO_2, CH_4, N_2O, and N_2 on MOF-5, MOF-177 and Zeolite 5A. *Environ. Sci. Technol.* **2010**, *44*, 1820−1826. (b) Zhao, Z.; Li, Z.; Lin, Y. S. Adsorption and diffusion of carbon dioxide on metal−organic framework (MOF-5). *Ind. Eng. Chem. Res.* **2009**, *48*, 10015−10020. (c) Silva, J. A. C.; Schumann, K.; Rodrigues, A. E. Sorption and

DOI: 10.1021/acs.inorgchem.8b00304
Inorg. Chem. XXXX, XXX, XXX−XXX

kinetics of CO_2 and CH_4 in binderless beads of 13X zeolite. *Microporous Mesoporous Mater.* **2012**, *158*, 219−228.
(15) Iota, V.; Yoo, C.-S. Phase diagram of carbon dioxide: evidence for a new associated phase. *Phys. Rev. Lett.* **2001**, *86*, 5922−5925.
(16) Valenzano, L.; Civalleri, B.; Chavan, S.; Palomino, G. T.; Areán, C. O.; Bordiga, S. Computational and experimental studies on the adsorption of CO, N_2, and CO_2 on Mg-MOF-74. *J. Phys. Chem. C* **2010**, *114*, 11185−11191.
(17) Vaidhyanathan, R.; Iremonger, S. S.; Shimizu, G. K. H.; Boyd, P. G.; Alavi, S.; Woo, T. K. Competition and cooperativity in carbon dioxide sorption by amine-functionalized metal−organic frameworks. *Angew. Chem., Int. Ed.* **2012**, *51*, 1826−1829.

DOI: 10.1021/acs.inorgchem.8b00304
Inorg. Chem. XXXX, XXX, XXX−XXX